Reaction dynamics of O(^1D) with HCN(0 0^0 v_3)

Christoph Kreher, Robert Theinl, and K.-H. Gericke
Institut für Physikalische und Theoretische Chemie der Johann Wolfgang Goethe-Universität, Marie-Curie-Strasse 11, D-60439 Frankfurt/Main, Germany

(Received 24 May 1994; accepted 15 August 1995)

The quantum state resolved reaction dynamics of HCN(0 0^0 v_3) with O(^1D) atoms were investigated by analyzing the complete product state distributions of OH($X\ ^2\Pi_\Omega, v, J$) and CN($X\ ^2\Sigma^+, v, J$) using laser induced fluorescence (LIF). The influence of the CH-stretching mode on the reaction dynamics and different branching ratios was inspected by exciting HCN to its first overtone band of the ν_3 CH stretch in the 1.5 μm region. The oxygen atom in the ^1D state was generated in a laser photolysis of ozone at a wavelength of 266 nm. The measured rotational and vibrational distributions of the products were compared with statistical results from phase space theory (PST). Nearly statistical rotational and vibrational distributions are obtained for CN($X\ ^2\Sigma^+$) in $v=0$–3. The rotational and vibrational distributions of OH($X\ ^2\Pi_\Omega$) are colder than statistically expected. Insertion of O into the CN bond with subsequent hydrogen migration seems to be a better characterization of the the reaction mechanism than an insertion of the oxygen atom into the CH bond. Direct abstraction of hydrogen to form OH is improbable to describe the molecular process. © *1995 American Institute of Physics.*

I. INTRODUCTION

Measuring nascent internal state distributions of products is a highly informative means of inspecting molecular reaction dynamics. The reaction of O with HCN is of interest because not only does it play an important role in combustion systems,[1] but also having several product reaction channels with products accessible by LIF or REMPI. The reaction can be divided into reactions involving ground-state oxygen atoms, O(^3P), and electronically excited oxygen atoms in the ^1D state.

The spin allowed reactions of oxygen in the triplet state are[2]

$$\mathrm{HCN}(\tilde{X}\ ^1\Sigma^+) + \mathrm{O}(^3P) \rightarrow \mathrm{H}(^2S_{1/2}) + \mathrm{NCO}(\tilde{X}\ ^2\Pi) \quad \Delta_r H^{298} = -25 \ \text{kJ/mol}, \tag{1}$$

$$\rightarrow \mathrm{NH}(X\ ^3\Sigma^-) + \mathrm{CO}(X\ ^1\Sigma^+) \quad \Delta_r H^{298} = -146 \ \text{kJ/mol}, \tag{2}$$

$$\rightarrow \mathrm{OH}(X\ ^2\Pi) + \mathrm{CN}(X\ ^2\Sigma^+) \quad \Delta_r H^{298} = +75 \ \text{kJ/mol}. \tag{3}$$

Previous gas phase studies[3,4] have determined that reaction (1) is the dominant channel, followed by channel (2). Channel (3) becomes important at higher collision energies. The reaction dynamics is characterized by an intermediate of HC(O)N, arising from O(^3P) addition to the CN–π bond of HCN, with subsequent dissociation to H and NCO. In the case of channel (2), a further intermediate, HNCO, is predicted. The total rate constant for the reaction system O(^3P)/HCN at 300 K was calculated from kinetic data by Perry[3] to be $k = 9.4 \times 10^{-18}\ \mathrm{T}^2\ e^{-E/\mathrm{RT}}$ with $E=28.45$ kJ/mol.

The possible spin allowed reaction channels for O(^1D)+HCN are[5]

$$\mathrm{HCN}(\tilde{X}\ ^1\Sigma^+) + \mathrm{O}(^1D) \rightarrow \mathrm{H}(^2S_{1/2}) + \mathrm{NCO}(\tilde{X}\ ^2\Pi) \quad \Delta_r H^{298} = -197 \ \text{kJ/mol}, \tag{4}$$

$$\rightarrow \mathrm{NH}(a\ ^1\Delta) + \mathrm{CO}(X\ ^1\Sigma^+) \quad \Delta_r H^{298} = -195.3 \ \text{kJ/mol}, \tag{5}$$

$$\rightarrow \mathrm{NH}(b\ ^1\Sigma^+) + \mathrm{CO}(X\ ^1\Sigma^+) \quad \Delta_r H^{298} = -92.0 \ \text{kJ/mol}, \tag{6}$$

$$\rightarrow \mathrm{OH}(X\ ^2\Pi) + \mathrm{CN}(X\ ^2\Sigma^+) \quad \Delta_r H^{298} = -99.6 \ \text{kJ/mol}, \tag{7}$$

$$\rightarrow \mathrm{OH}(X\ ^2\Pi) + \mathrm{CN}(A\ ^2\Pi) \quad \Delta_r H^{298} = +10.9 \ \text{kJ/mol}. \tag{8}$$

There are several studies on the dynamics of the reaction O(^1D)+HCN, examining the kinetics as well as the product state distributions. Carpenter *et al.*[5] have shown that the main channels for deactivation of O(^1D) by HCN are reactions (5) and (7), of which reaction (5) is much more dominant with a ratio of the rate coefficients $k_5/k_7 \approx 9$. The possible spin allowed reaction channels producing NO+CH or C+HNO are significantly endothermic and are not further discussed.

In this paper the products OH($X\ ^2\Pi$) and CN($X\ ^2\Sigma$) of the reaction channel (7) were monitored by the laser induced fluorescence technique (LIF).[6,7] Furthermore, the influence of vibrational motion in HCN on the reaction dynamics is investigated by ir excitation of the first overtone band of the C–H stretching mode[8–13]

$$\mathrm{HCN}(J=8, v_1=0, v_2=0, v_3=0) + h\nu(1.53\ \mu\mathrm{m}) \rightarrow \mathrm{HCN}(J'=9, v_1'=0, v_2'=0, v_3'=2). \tag{9}$$

Spectroscopic studies of hydrogen cyanide acid have been performed by many research groups because of its significance in chemical physics and astrophysics. The (0 0^0 2)←(0 0^0 0) overtone band of HCN has a large band inten-

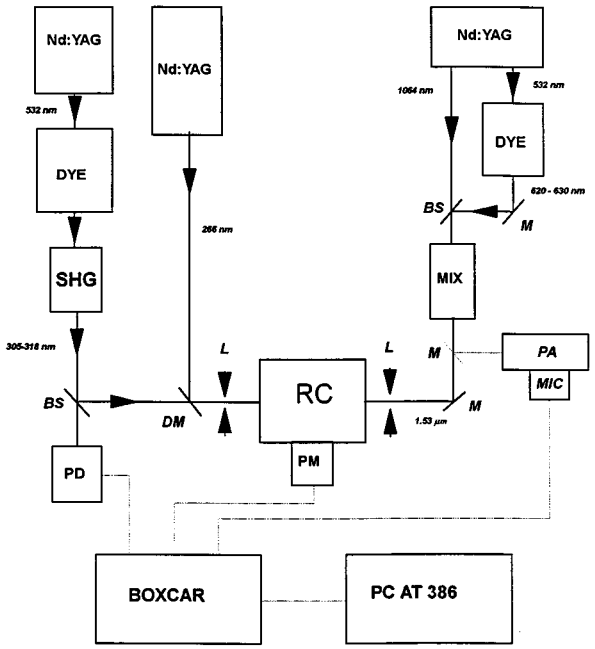

FIG. 1. Schematic drawing of the experimental setup. (RC=reaction chamber, PM=photomultiplier, PA=photoacoustic cell, MIC=microphone, L=lens, SHG=second harmonic generator, M=mirror, BS=beam splitter, DM=dicroitic mirror, PD=photodiode, DYE=dye laser, MIX=frequency mixing.

sity of 8.5×10^4 cm/mol.[10] Using the Avogadro number we calculate an integrated absorption cross section of $\sigma_0=5.0\times10^{-21}$ cm for the chosen molecular transition.

II. EXPERIMENT

HCN gas was prepared by reaction of NaCN with H_2SO_4.[14,15] Subsequent distillation over $CaCl_2$ and P_2O_5 removed possible water residues. Oxygen atoms in the ^1D state were generated from ozone in a pulsed laser photolysis. By firing the fourth harmonic of a Nd-YAG laser (Quanta-Ray DCR 1A) into the cell, the focused output generated $O(^1D)+O_2(^1\Delta_g)$.[16,17] Ozone was prepared in a silent discharge in O_2 (99.95% purity).[18,19] To avoid any reactions of O_3 with HCN prior to photolytic initiation, the reactants were mixed in the reaction chamber by separate nozzles. The chamber was evacuated by an oil diffusion pump, reaching a base pressure of $\sim10^{-2}$ Pa. The partial pressures were $P_{O_3}=4$ Pa and $P_{HCN}=6$ Pa. The experimental setup is shown in Fig. 1.

Probing the $(0\ 0^0\ 2)\leftarrow(0\ 0^0\ 0)$ overtone band of HCN in the infrared region was performed via difference frequency mixing of a dye laser and a 1.064 μm Nd-YAG laser beam (Continuum YG 680, TDL 60, IRP). The dye laser operated with DCM at an output energy of 80 mJ at 627 nm. The beams were mixed in a lithium niobate crystal and an automatic wavelength tracking system was used to maintain the optimum conversion efficiency if the laser was tuned. The ir output at 1.5 μm was separated from the residual radiation at 627 nm and 1.064 μm by a CaF_2 Pellin Broca prism and focused into the interaction region of the cell with a 65 cm planoconvex lens. The beam diameter in the focal region was $\approx$0.4 mm. At a pulse energy of 15 mJ a photon flux of $\approx9.0\times10^{19}$ photons/cm^2 is achieved.

We excited the $(0\leftarrow0)$, $(1\leftarrow1)$, $(2\leftarrow2)$, $(0\leftarrow2)$, and $(1\leftarrow3)$ vibrational bands of the $A\ ^2\Sigma^+\leftarrow X\ ^2\Pi$ transition of OH. The LIF-probe beam at wavelengths around 305–320 nm was generated using the frequency doubled output of a Nd-YAG pumped dye laser (Quantel TDL IV) operated with DCM at a pulse energy of $\sim$100 μJ. The CN product state distribution was probed by an excimer pumped dye laser (Lambda Physik EMG 101 MSC and FL 2002). The dye laser was operated with QUI in the region of 375 to 390 nm. All LIF spectra were detected under saturated conditions. The lasers were operated with a repetition rate of 10 Hz. The time delay between the photolysis laser—which is in time with the ir probe laser—and the LIF-probe laser was set to 150 ns for CN and 300 ns for OH. The LIF signal was monitored with a photomultiplier (THORN-EMI 9781B). To reduce scattered light from the laser beams, the LIF signal was spectrally filtered by an interference filter of known transmission. Furthermore the reaction chamber was equipped with 50 cm sidearms which contained baffles.

A separate photoacoustic cell, 12 cm in length, was used for controlling the spectral overlap between the narrow absorption lines of HCN ($\Delta\nu\approx0.016$ cm^{-1}) and the ir laser light ($\Delta\nu_l\approx0.1$ cm^{-1}).[9] The cell was equipped with CaF_2 Brewster windows at both ends. We used a commercially available microphone to detect the photoacoustic signal. The spectral width of the ir light was obtained by measuring the linewidth (FWHM) of a HCN transition. The cross section σ for excitation of HCN via the $R(8)$ line is $\sigma\approx\sigma_0/\Delta\nu_l\approx5.0\times10^{-20}$ cm^2. The high intensity of the ir laser in the focal region, $I=0.9\times10^{20}$ photons/cm^2,[2] guarantees saturation of the HCN transition.

III. RESULTS

A. OH product state distribution

The LIF-spectra observed via reaction (7) are shown in Figs. (2) (OH) and (3) (CN). OH($X\ ^2\Pi$) was detected by exciting the 0–0 and 1–1 band of the $A\ ^2\Sigma^+\leftarrow X\ ^2\Pi$ transition. No LIF signal was observed, when the vibrational bands (2–2), (0–2), and (1–3) of OH were probed in the wavelength region 318–322 and 390–394 nm. Thus OH($X\ ^2\Pi$) is only generated in the two lowest vibrational states. The vibrational distribution of OH is $P(v=1)/P(v=0)=0.14\pm0.02$, thus only a small quantity of OH is produced in $v=1$.

Figure 4 represents the rotational distribution of OH($X\ ^2\Pi_\Omega$, $v=0,1$) as a Boltzmann plot. The distributions can approximately be characterized by Boltzmann temperatures. We found rotational temperatures of (3090 ± 90) K for $\Pi_{3/2}(v=0)$ and (3270 ± 140) K for $\Pi_{1/2}(v=0)$. For the vibrationally excited state of OH the rotational distribution can be described by the temperatures of (2000 ± 170) K and (2310 ± 140) K for the $\Pi_{3/2}$ and $\Pi_{1/2}$ states, respectively. Although the temperatures are slightly different for the two spin orbit systems, no deviation from a statistical population of the two spin states $^2\Pi_{3/2}$ and $^2\Pi_{1/2}$ is observed. The observed popu-

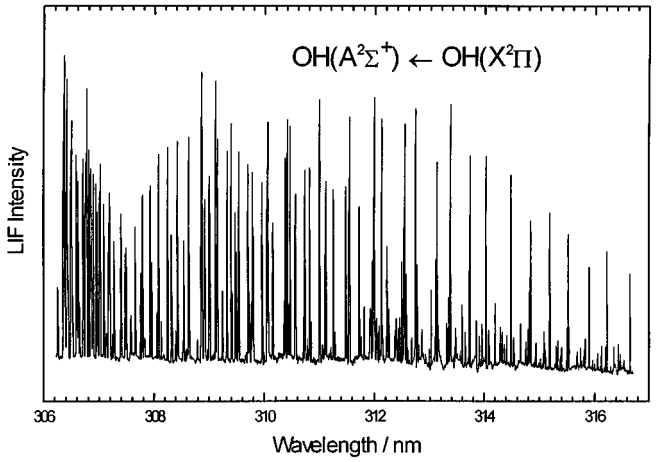

FIG. 2. Nascent LIF spectra of the 0–0 and 1–1 band of the OH($A\ ^2\Sigma^+$)—OH($X\ ^2\Pi$) transition between 306 and 317 nm. The OH(X) products are generated in the reaction of thermal HCN with O(^1D).

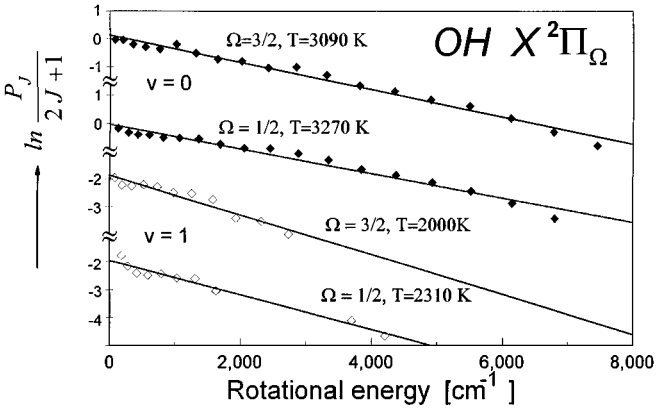

FIG. 4. Boltzmann plot of the rotational distribution, characterizing the $\Omega=3/2$ and $\Omega=1/2$ spin orbit systems of OH($X\ ^2\Pi_\Omega, v=0,1$). The lines represent least square fits to a Boltzmann distribution. Open squares represent $v=0$ and solid squares refer to $v=1$. Units of the Y axis are relative. The axis is broken (≈mark) for a better comparison of the rotational distribution.

lation ratio is $P_{\Pi_{3/2}}/P_{\Pi_{1/2}} = 1.09 \pm 0.23$ for $v=0$ and $P_{\Pi_{3/2}}/P_{\Pi_{1/2}} = 0.94 \pm 0.24$ for $v=1$. Appropriate statistical weights have been considered.

The second electronic fine structure of OH molecules is the Λ doubling which arises from the interaction between nuclear rotation and orbital angular momentum. At high angular momentum the two levels have opposite symmetry, $\Pi(A')$ and $\Pi(A'')$, with respect to reflection in the plane of rotation. Since each of the two Λ components of OH is probed by different rotational branches, Λ-doublet partitioning is obtained by a comparison of the LIF intensities for P/R lines, probing the $\Pi(A')$ component, with those of corresponding Q lines, probing the $\Pi(A'')$ component. No significant preference in the population of the Λ doublets is observed (Fig. 5). No accurate determination of the Λ doublet distribution in OH($v=1$) was possible due to spectral overlap of some relevant transitions.

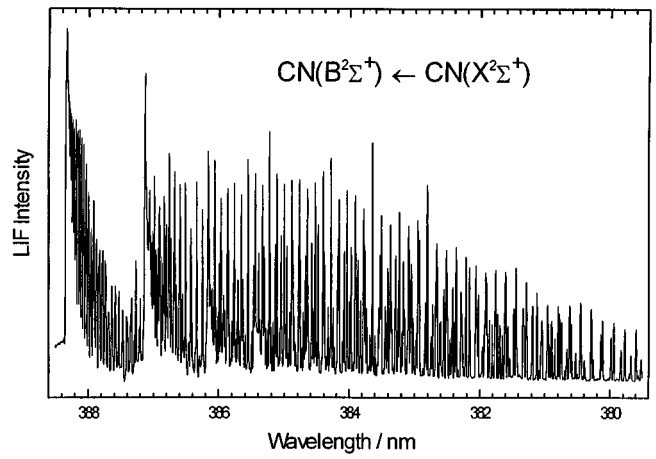

FIG. 3. Nascent LIF spectra of the $B\ ^2\Sigma^+ - X\ ^2\Sigma^+$ transition of CN. The CN(X) products are generated in the reaction of thermal HCN with O(^1D).

B. CN product state distribution

The rotational state distributions of CN ($v=0$–3) from reaction (7) are depicted in Fig. 6 as Boltzmann plots. The distributions for $v=0$ and 1 are characterized by a low temperature ($T_{v=0}=390$ K, $T_{v=1}=400$ K) component at low rotational states and a high temperature ($T_{v=0}=5000$ K $J>17$, $T_{v=1}=4200$ K $J>10$) component at higher rotational levels. These observations can be explained by effects of rotational relaxation. Because of the small energy gap between the rotational levels at low J, the rotational relaxation should be very effective for these levels. The fraction of CN fragments that are relaxed by collisions is ~6%. Assuming a gas kinetic collision rate we calculated a value of ~4% of those CN fragments, which have collided with HCN at least once within the time delay of 150 ns. This is in agreement with the experiment. The rotational temperatures for CN($X\ ^2\Sigma^+$) in $v=2$ and $v=3$ are (2990±100) K and (1570 ±80) K.

The CN products are formed in the vibrational states $v=0$–3 with population ratios of $P(v=0)/P(v=1)/P(v=2)/P(v=3)=0.45{:}0.29{:}0.18{:}0.08$. We estimate the upper

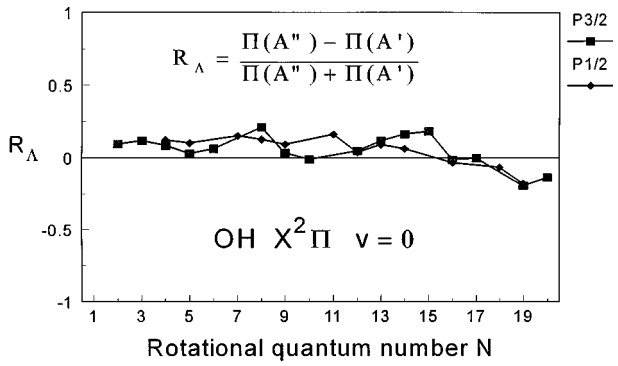

FIG. 5. Λ-state distribution for the OH fragment in $v=0$. Different symbols for the two spin states are used.

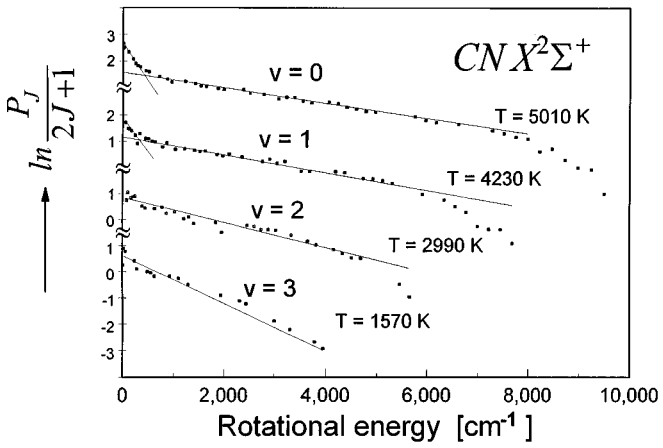

FIG. 6. Boltzmann plot of the rotational distribution of CN($X\ ^2\Sigma^+, v=0-3$) from the reaction of thermal HCN with O(^1D). The lines represent the best fits to Boltzmann distributions. Units of the Y axis are relative. The axis is broken ("≈") for a better comparison of the rotational distribution.

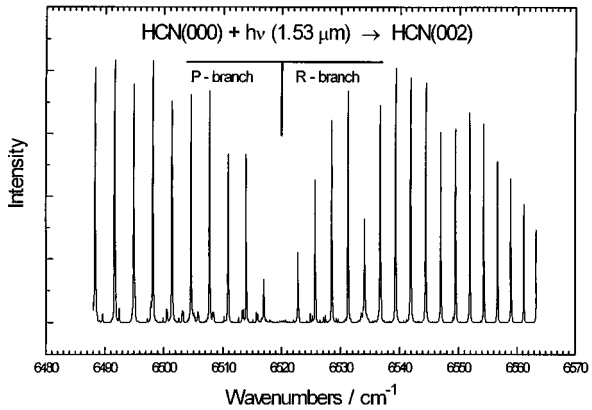

FIG. 7. Photoacoustic spectra of the $\tilde{X}\ ^1\Sigma^+(v_3'=2,\ J')\leftarrow\tilde{X}\ ^1\Sigma^+(v_3=0,\ J)$ transition of HCN. Since HCN is a linear molecule, the ir spectrum consists of a P and R branch.

limit of the population of CN in $v=4$ from the noise level to be <0.02.

C. H+NCO channel

The possible production of NCO($\tilde{X}\ ^2\Pi$) from reaction (4) was investigated by probing the $\tilde{B}\ ^2\Pi\leftarrow\tilde{X}\ ^2\Pi$ transition of NCO in the region 300–320 nm. No laser induced fluorescence was detected. From the different partitioning functions of NCO and OH and from the S/N ratio of the spectra we estimate an upper limit for the branching ratio, $k_4/k_7\leqslant 0.5$.

D. Influence of vibrationally excited HCN(0 0^0 2)

The excitation of HCN into its first overtone band of v_3 by an ir laser beam at 1.53 μm was checked by using photoacoustic spectroscopy. The $\tilde{X}\ ^1\Sigma^+(v_3'=2,\ J')\leftarrow\tilde{X}\ ^1\Sigma^+(v_3=0,\ J)$ spectra of HCN shows P and R lines according to $J'=J-1$ and $J'=J+1$. Because of the low symmetry of HCN($\tilde{X}\ ^1\Sigma^+$), the lines can easily be assigned to their transitions. Figure 7 shows the high resolution spectra of the (0 0^0 2)←(0 0^0 0) overtone band in the wavelength region of 6488–6564 cm^{-1}. In order to maximize the amount of excited HCN, we used the $J'=9\leftarrow J=8$ rotational transition at 6544.31 cm^{-1}. The excitation was performed under saturation conditions.

The experiments with vibrationally excited HCN were performed by using a trigger-suspending device which triggered the Q switch of the Nd-YAG laser used in the ir package on every second pulse. Within a single scan, we obtained two data sets, one with HCN($v_3=0$) and another with HCN($v_3=2$, $J'=9$). A very precise evidence on the influence of HCN($v_3=2$) is given by the difference of both data sets.

No effects of additional excitation of HCN into its (0 0^0 2) vibrational state on the reaction dynamics of O(^1D)+HCN was observed. Although the available energy is increased by ~79 kJ/mol, no increase of the LIF signal was observed. A reason for that could be the low portion of HCN which can be excited by the ir-probe beam. With the rotational constant for HCN, $B=1.478$ cm^{-1}, and in case of complete saturation of the transition we calculated the highest amount of excited HCN molecules (R line) according to

$$\frac{n(J)}{N}=\frac{1}{2}\cdot\frac{2J+3}{2J+1}\cdot\frac{2J+1}{q_{\rm rot}}\cdot e^{-[BhcJ(J+1)]/[kT]}. \qquad (10)$$

For ($J'=9\leftarrow J=8$) only 4% of all HCN molecules are in the excited (0 0^0 2) state. We also tried to monitor OH in the second vibrational state where no products are generated by the "thermal reaction." However, no lines in the region of the $A\ ^2\Sigma^+(v'=0)\leftarrow X\ ^2\Pi(v=2)$ transition could be observed.

IV. DISCUSSION

The rotational state distribution of CN observed in our experiments shows considerable differences to the results of Carpenter *et al.* Although their O_3 photolysis was performed at 248 nm—the available energy $E_{\rm av}$ for the products is about 15.9 kJ/mol higher—the observed rotational distributions of CN in $v=0$, 2, and 3 were significantly colder. Furthermore, Carpenter observed in the vibrational state $v=1$ of CN a rotational distribution, which could be described by two temperatures; a lower temperature of ~1000 K and a temperature near 6000 K of higher rotational levels. The break in the observed population distribution was explained by a minor channel leading to the production of vibrationally excited OH($v>1$). Nascent OH product state distributions were not obtained due to strong background chemiluminescence. In the present experiment we observe no chemiluminescence and the complete OH distribution is determined. Due to the facts that we did not observe OH products in $v>1$ and that the rotational relaxation of CN products is very fast it may be possible that the break of population could be an effect of relaxation. It is unlikely that the different O(^1D) translational energy is responsible for a bimodal rotational distribution in only one vibrational state.

TABLE I. Vibrational product state distribution, mean rotational and vibrational energies of the reaction products.

Product	Vibrational level	$P(v)$ PST	$P(v)$ Experiment	$\langle E_{\rm rot}(v)\rangle$ kJ mol^{-1}	$\langle E_{\rm vib}(v)\rangle$ kJ mol^{-1}
OH	0	0.69	0.88	23.17	0
	1	0.25	0.12	1.27	4.85
	sum	0.94	1.0	24.44	4.85
CN	0	0.47	0.45	17.36	0
	1	0.28	0.29	7.20	7.08
	2	0.15	0.18	3.01	8.74
	3	0.07	0.08	0.76	5.79
	sum	0.97	1.0	28.33	21.61

A. Product energies

The available energy $E_{\rm av}$ is partitioned among the degrees of freedom of the reaction products OH and CN. $E_{\rm av}$ is given by

$$E_{\rm av}=-\Delta_r H^0+E_{\rm int}({\rm HCN})+\Delta E_{\rm coll}. \tag{11}$$

At room temperature $E_{\rm int}$(HCN) includes only the rotational energy of HCN; $E_{\rm int}$(HCN)=RT=2.5 kJ/mol. The collision energy $\Delta E_{\rm coll}$ is calculated by

$$\Delta E_{\rm coll}=\frac{1}{2}\,\mu_{\rm O,HCN}\cdot v_{\rm rel}^2=\tfrac{1}{2}\mu_{\rm O,HCN}(\overline{v_{\rm O_3}^2}+\overline{v_{\rm HCN}^2}+\overline{v_{\rm Ocm}^2}). \tag{12}$$

$\overline{v_{\rm O_3}^2}$ and $\overline{v_{\rm HCN}^2}$ can be calculated by the equation $\overline{v^2}=3RT/m$ and $\overline{v_{\rm Ocm}^2}$ by the equation

$$\overline{\mathbf{v}_{\rm Ocm}^2}=\frac{1}{m_{\rm O}^2}\,2E_t({\rm O,O_2})\mu_{\rm O,O_2}. \tag{13}$$

The translational center-of-mass energy, E_t(O,O$_2$), of O(^1D) and O$_2$ from ozone photolysis at 266 nm was determined by Sparks *et al.*[20] to be 54.4 kJ/mol. With the reaction enthalpy of $\Delta_r H^0=-99.6$ kJ/mol the average available energy for the products OH and CN is ~127 kJ/mol. For the reaction of ir selected HCN($J'=9$, $v_3=2$) the available energy is ~206 kJ/mol.

The mean rotational energies for OH and CN were calculated by the equation

$$\langle E_{\rm rot}\rangle=\sum_v\,\langle E_{\rm rot}\rangle_v=\sum_{v,J}\,P_v(J)E_{\rm rot}(J), \tag{14}$$

where $P_v(J)$ is the rotational state distribution and $E_{\rm rot}(J)$ is the rotational energy of a rotational state in a selected vibrational state. The mean vibrational energy is given by

$$\langle E_{\rm vib}\rangle=\sum_v\,P(v)E_{\rm vib}(v), \tag{15}$$

where $P(v)=\Sigma_J P_v(J)$ is the population of each vibrational state v, $\Sigma_v P(v)=1$, and $E_{\rm vib}(v)$ is the energy of the vibrational state.

The average rotational and vibrational energies of OH from Eqs. (14) and (15) are $\langle E_{\rm rot}\rangle$=24.44 kJ/mol and $\langle E_{\rm vib}\rangle$=4.85 kJ/mol. For CN we obtain $\langle E_{\rm rot}\rangle$=28.33 kJ/mol and $\langle E_{\rm vib}\rangle$=21.61 kJ/mol. The translational center-of-mass energy of the products, E_{trans}, is obtained from the conservation of energy according to

$$\langle E_{trans}\rangle=E_{\rm av}-\langle E_{\rm rot}({\rm OH})\rangle-\langle E_{\rm vib}({\rm OH})\rangle-\langle E_{\rm rot}({\rm CN})\rangle-\langle E_{\rm vib}({\rm CN})\rangle. \tag{16}$$

47.77 kJ/mol or 38% of the available energy is allocated to translational motion of the products, OH and CN. The results and the respective partition numbers $f_i=\langle E_i\rangle/E_{\rm av}$ are shown in Tables I and II.

Different reaction pathways have to be considered in order to explain the experimental observations: The attacking oxygen atom may simply abstract the hydrogen atom, the OH and CN products may be formed by an insertion of O(^1D) into the H–C bond or by an insertion of O(^1D) into the CN bond with subsequent migration of the H atom.

A direct abstraction of an H atom by O(^1D) has already been observed in reactions between O(^1D) and alkanes [C_3H_8, $CH(CH_3)_3$].[21] However, in that case the CN product should show very low internal excitation because it acts as a spectator during the reaction process. On the other hand, the OH product should be highly vibrationally excited, but no high rotational levels should be populated. Excitation of the v_3 stretch in HCN should even prefer the formation of OH in high vibrational states. For a sensitive detection of OH in $v=2$ $A\ ^2\Sigma^+(v'=0)\leftarrow X\ ^2\Pi(v=2)$ transition around 392 nm is excited using an excimer pumped dye laser with a QUI dye solution and observing the fluorescence of the $v'=0\rightarrow v=0$ band. Scattered light from the probe laser is discriminated by an interference filter. We could not find any lines according to the $A\ ^2\Sigma^+(v'=0)\leftarrow X\ ^2\Pi(v=2)$ transition of OH. The sensitivity of the OH($v=2$) detection was

TABLE II. Partitioning of the available energy ($E_{\rm av}$=127 kJ/mol) into the vibrational, rotational and translational degrees of freedom of OH and CN.

	Energy (kJ mol^{-1})	$f_i=E_i/E_{\rm av}$	f_i PST
$E_{\rm rot}$ (CN)	28.33	0.22	0.19
$E_{\rm vib}$ (CN)	21.61	0.17	0.17
$E_{\rm rot}$ (OH)	24.44	0.19	0.25
$E_{\rm vib}$ (OH)	4.85	0.04	0.12
E_{trans} (OH,CN)	47.77	0.38	0.27
sum	127.0	1.0	1.0

checked by adding an equivalent amount of O_3/H_2O into the reaction cell. The reaction of O(^1D) and H_2O produces vibrational excited OH with 9% of the OH in $v=2$. From the S/N ratio of the spectra when using H_2O or HCN, we estimate that in the reaction of O(^1D) with HCN(0 0^0 2) less than 4% of the OH products are generated in $v=2$. Although only 4% of HCN are vibrationally excited, the signal to noise ratio is sufficient to observe OH($v=2$) if it were generated via HCN(v)+O(^1D) in a significant amount [$P(v=2)\geqslant 0.04$] because the reaction of "thermal" HCN reactants leads only to OH in $v=0,1$ state. Since all experimental observations contradict the expectations of an abstraction mechanism, this type of reaction can be ruled out.

Also a "head on" collision of O(^1D) on the H atom of HCN seems to be very unlikely because the rotational excitation of CN should be low and no significant vibrational excitation of the stiff CN bond can be expected.

Quite often an insertion of the O(^1D) atom into an H–R bond is observed which leads to OH products via the H–O–R intermediate. A prototype of this reaction is the process $O(^1D)+H_2\rightarrow OH(v,J)+H$,[18,22] where the collision complex is H_2O with high excitation of the bending motion. When sufficient energy flows into a H–OH bond so that this bond will break, then the remaining energy will essentially be released as rotation.

In case of an insertion of O(^1D) into the H–CN bond followed by a direct decay into HO and CN one would also expect highly rotationally excited OH products. The CN rotation should also be excited, but significantly lower than that of OH. The OH vibrational excitation is expected to be low and that of the CN product should be even lower. Although OH is formed in high rotational states with low vibrational excitation, the CN product state distribution disagrees with the picture of a direct reaction where O(^1D) is inserted into the H–C bond followed by a fast break of the HO–CN bond.

In general, one assumes that a direct and fast reaction leads to a vibrationally excited "new" bond (OH) while the "old" bond (CN) already existing in the reactant (HCN) remains essentially unaffected, i.e., a low vibrational excitation of CN is expected. Since CN is generated with a significant amount of vibration, a direct reaction of O(^1D)+HCN seems to be very unlikely. Insertion of the O(^1D) atom into the H–CN bond can only explain the experimental observations when the HOCN intermediate lives long enough to ensure sufficient internal energy transfer into the CN bond.

Another explanation of the reaction dynamics may be an insertion of the O(^1D) atom into the CN bond leading to an oxazirine intermediate

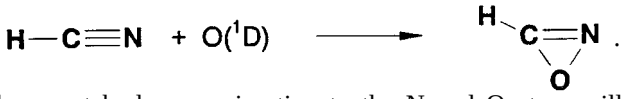

Subsequent hydrogen migration to the N and O atom will form HNCO and HOCN, respectively. The dissociation of these intermediates leads to the fragments NH+CO [reaction (5)],

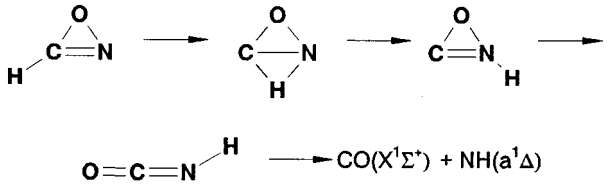

(17)

and OH+CN [reaction (7)]

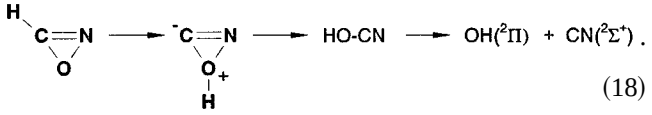

(18)

Such a collision complex has to live longer than a vibrational period before it can decay into OH and CN products because a migration of the hydrogen atom is necessary.

A long living complex implies randomization of energy. Thus it is very useful to investigate the reaction using phase space theory (PST).[23–25] In the following we will compare our experimental results with completely statistical distributions. The phase space theory assumes that the reaction complex will dissociate with equal probability into each of the accessible product channels, therefore enabling a statistical partitioning of the available energy into the product states. Accessible channels are those that satisfy the laws of conservation of energy and angular momentum between reactants and products. The PST is therefore more precise than the prior distribution, which only satisfies the law of conservation of energy. A detailed discussion about these statistical theories has been carried out by Ben-Saul.[26]

The conservation of angular momentum for the reaction $O(^1D)+HCN\rightarrow OH+CN$ can be written by $\mathbf{J}=\mathbf{J}_O+\mathbf{J}_{HCN}+\mathbf{L}=\mathbf{J}_{OH}+\mathbf{J}_{CN}+\mathbf{L}'$, where $\mathbf{J}$ is the total angular momentum and $\mathbf{L}$ (or $\mathbf{L}'$) is the orbital angular momentum of the reactants (or products). PST assumes that all accessible states have equal weight and the probability to find the products in the rotational states J_{OH} and J_{CN} with given J is equal to the number of allowed values of L'. We calculate this number by counting over all allowed angular momentum vectors L', that are given by the so-called triangle condition, $|J'-J_{CN}|\leqslant L'\leqslant(J'+J_{CN})$ with $J'=J_{CN}+L'$. Conservation of angular momentum implies the restriction of J' analogous to L' according to $|J-J_{OH}|\leqslant J'\leqslant(J+J_{OH})$. For given values of J, J_{OH}, and J_{CN}, the probability $P:=P(J,J_{OH},J_{CN})$ is obtained by summing over L' and J'

$$P(J,J_{OH},J_{CN})=(2J+1)\sum_{J'}\sum_{L'}\begin{cases}1, & L'\leqslant L'_{max}\\ 0, & L'>L'_{max}\end{cases}.$$

The constraint $L'\leqslant L'_{max}$ is related to the dynamics of the separating fragments described by Pechukas[23] and is given as follows:

$$L'(L'+1)\hbar^2\leqslant 6\mu' C_6^{1/3}\left(\frac{1}{2}E_T\right)^{2/3}. \tag{19}$$

E_T is the translational energy of the products OH and CN, μ is the reduced mass and C_6 is the coefficient of the asymptotic expression for the attractive part (r^{-6}) of the potential

between the products. Using a Lennard-Jones potential as in Ref. 27 we estimate C_6 to be 2.2×10^{-78} Jm^6. Setting $L'(L'+1)\approx L'^2$ we obtain the upper limit of the orbital angular momentum L' (E_T in kJ/mol)

$$L'_{\max}\approx 34\hbar\cdot\sqrt[3]{E_T}. \tag{20}$$

The probability of forming a reaction complex from the initial state J_O, J_{HCN}, L is given by

$$\frac{1}{(2J_O+1)(2J_{HCN}+1)(2L+1)},$$

if $|J''-L|\leqslant J\leqslant(J''+L)$ and $|J_O-J_{HCN}|\leqslant J''\leqslant(J_O+J_{HCN})$, otherwise it is zero.[24]

For given values of J_O, J_{HCN} and L, the probability to find the products in the rotational states J_{OH} and J_{CN}, is now obtained by summing over all J and J''

$$P(J_O,J_{HCN},L,J_{OH},J_{CN})\propto\frac{(2L+1)\Sigma_{J''}\Sigma_J P(J,J_{OH},J_{CN})}{(2J_O+1)(2J_{HCN}+1)(2L+1)}. \tag{21}$$

The next step is the summation over all possible J_O, J_{HCN} and L

$$P(J_{OH},J_{CN})\propto\sum_{J_{HCN}}\sum_{L}P(J_O=2,J_{HCN},L,J_{OH},J_{CN})\times f(J_{HCN})f(L). \tag{22}$$

A summation of the rotational angular momenta of the oxygen atom is not necessary, because of $J_O=2$. $f(J_{HCN})$ is the fraction of HCN in the quantum state J which is given by the Boltzmann distribution

$$f(J_{HCN})=(2J_{HCN}+1)e^{-[E(J_{HCN})]/[kT_{300\ K}]}. \tag{23}$$

The orbital momentum L is constrained by a maximum angular momentum according to

$$f(L)=\begin{cases}1, & L\leqslant L_{\max}\\ 0, & L>L_{\max}.\end{cases}$$

$P(J_{OH},J_{CN})$ in Eq. (22) is the joint reaction probability of formation of OH in a specific state J_{OH}, while the partner product CN is formed in the J_{CN} state. The product state distribution which is observed in the present experiment of one product is obtained by summation over all states of the partner product where conservation of energy has to be considered. The rovibrational state distribution of CN is given by

$$P(\nu_{CN},J_{CN},E_{av})\propto\sum_{\nu_{OH}}\sum_{J_{OH}}P(J_{OH},J_{CN}), \tag{24}$$

where the vibrational quantum number v is explicitly used.

Equations (19)–(24) were developed into a suitable form for computer calculations. We neglected the rotational angular momentum of oxygen by setting $\mathbf{J}\approx\mathbf{L}+\mathbf{J}_{HCN}$ in order to decrease the computing time. The calculations were carried out with $E_{av}=127$ kJ/mol, $L\leqslant 90\hbar$ and $J_{HCN}\leqslant 30\hbar$. The orbital angular momentum $L'_{\max}$ was calculated by Eq. (20).

The rotational state distribution of CN in $v=0$–3 together with the statistical distribution arising from PST are shown in Fig. 8. For each vibrational level the rotational distribution up to high rotational energies can well be described by phase space theory (PST). The deviation from the experimental results are less than 10%. Figure 9 shows the vibrational distribution of the products OH and CN together with the state distribution from PST. The vibrational state population of CN can also be well described by phase space theory. Using PST one can estimate the upper limit of CN population in $v=4$ to ~2% and in $v=5$ to <0.1% which is in agreement with the experimental observations.

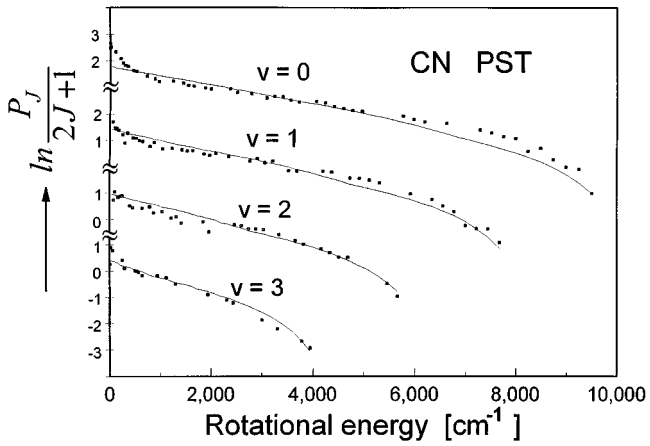

FIG. 8. CN($v=0$–3) product rotational distributions from PST (lines) and from experimental results (symbols). The agreement between both data sets is very good. Units of the Y axis are relative. The axis is broken ("≈") for a better comparison of the rotational distribution.

The statistical product state distribution of CN seems to suggests the presence of a long living reaction complex where complete internal energy randomization explains the reaction mechanism. However, the OH state distribution can not be described by phase space theory: In our experiment a distinct lower population in the rotational and vibrational states is observed (Figs. 9 and 10). While the OH rotational excitation is only slightly lower than statistically expected

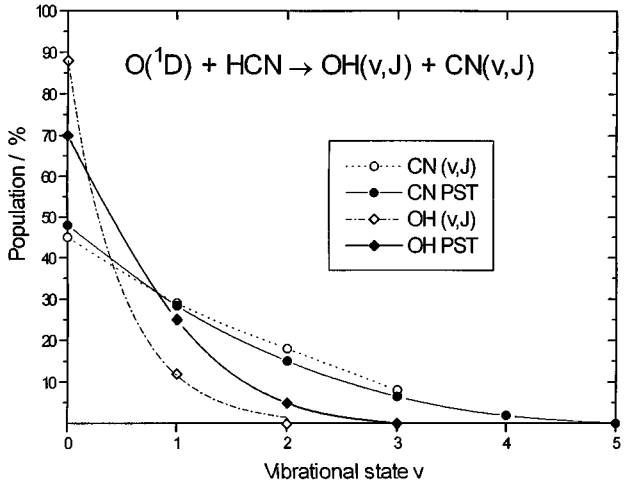

FIG. 9. Vibrational distributions of the products OH and CN. The dashed lines show the calculated using PST and the symbols represent the experimental data. While for CN the agreement is very good the behavior of the OH fragments can not be described with the statistical theory.

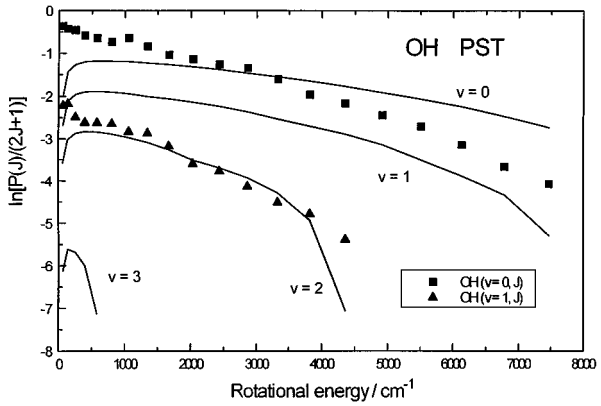

FIG. 10. Boltzmann plot of the rotational distribution of OH($X\ ^2\Pi$). The solid line represents the corresponding statistical distribution from PST.

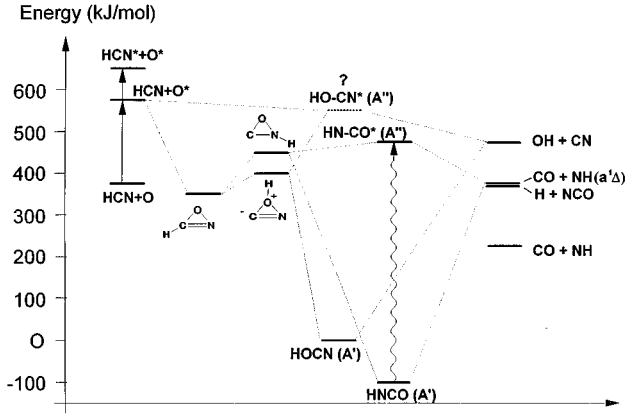

FIG. 11. Correlation diagram for the reaction of O(^1D)+HCN. The heats of formation of the reaction intermediates are taken from Poppinger *et al.* (Ref. 28). The state energies of HNCO(A')=−24.9 kJ/mol and HNCO(A'')=475 kJ/mol are taken from Ref. 29.

(Table II), the deviation of the vibrational excitation is much stronger. A statistical population of the OH fragments allows vibrational excitation up to $v=3$. Reaction (7) generates OH($X\ ^2\Pi$) only in the two lowest vibrational states. This analysis suggests that the reaction O(^1D)+HCN $\rightarrow$OH($X\ ^2\Pi$)+CN($X\ ^2\Sigma^+$) cannot completely be described by a statistical process. Specific dynamical effects have to be considered to characterize the state distribution of the OH products. Strong anisotropic forces in the exit channel of the reaction complex, for example, would transfer the available energy nonstatistically to the rotational and vibrational states of the OH($X\ ^2\Pi$) product, as observed in the current study.

In order to explain the reaction geometry we examined the Λ-state distribution of OH, which reflects the symmetry conservation in the reactive process. Reactants which are (anti)symmetric with respect to the point group of the collision geometry will be transformed to products which are also (anti)symmetric. By assuming the maintenance of planarity of the reaction path, the point group of the reaction complex will be C_s. Whether the reaction proceeds via the ground state surface A' or via the A'' surface of HOCN can in principle be answered by analyzing the Λ-state distribution of OH. The symmetric reactants O(^1D) and HCN($\tilde{X}\ ^1\Sigma^+$) yield a symmetric collision complex, HOCN(A'), that dissociates to symmetric products, OH[$^2\Pi(A')$] and CN($X\ ^2\Sigma^+$). However, reaction (18) can proceed via both surfaces A' and A'' of HOCN, which leads to OH populations observed in our experiment (Fig. 11). We could not find any significant preference for one of the two Λ states (A' and A'') of OH. Other reasons for that effect of low Λ selectivity could be nonadiabatic transitions in the exit channel and the transformation of electron orbital angular momentum into rotational angular momentum. Also a strong energy transfer into the degrees of freedom of the long lived reaction complex, especially into out-of-plane vibrational modes, causes equal preference of the Λ states.

In summary, a direct and fast reaction mechanism for the generation of OH and CN can be excluded. A long living reaction complex is formed by insertion of O(^1D) into either the H–C or the CN bond of HCN. Although the agreement of the statistical with the experimental CN distribution is excellent, the OH distribution implies that PST cannot rigorously be used to calculate the complete product state distribution and anisotropic forces in the exit channel of the reaction complex have to be considered to explain the reaction mechanism.

ACKNOWLEDGMENTS

This work was supported by the Deutsche Forschungsgemeinschaft. We thank Professor Dr. F. J. Comes for useful discussions and material support. C.K. thanks the Fonds der Chemischen Industrie for fellowship support.

[1] R. J. Cicerone and R. Zellner, J. Geophys. Res. **88**, 10689 (1983).
[2] J. N. Crowley and J. R. Sodeau, J. Phys. Chem. **93**, 3100 (1989).
[3] R. A. Perry and C. F. Melius, Proc. Symp. Combust. Int. **20**, 639 (1984).
[4] A. Szekely, R. K. Hansons, and C. T. Bowman, Proc. Symp. Combust. Int. **20**, 647 (1984).
[5] B. K. Carpenter, N. Goldstein, A. Kam, and R. J. Wiesenfeld, J. Chem. Phys. **81**, 1785 (1984).
[6] J. L. Kinsey, Ann. Rev. Phys. Chem. **28**, 349 (1978).
[7] W. Demtröder, *Laser Spectroscopy* (Springer, Berlin, 1982), p. 417.
[8] H. Sasada, J. Chem. Phys. **88**, 767 (1988).
[9] K. R. German and W. S. Gornall, J. Opt. Soc. Am. **71**, 1452 (1981).
[10] A. M. Smith, S. L. Coy, and W. Klemperer, J. Mol. Spectrosc. **134**, 134 (1989).
[11] D. H. Rank and G. Skrinko, J. Opt. Soc. Am. **50**, 421 (1960).
[12] A. M. Smith and U. G. Jørgensen, J. Chem. Phys. **87**, 5649 (1987).
[13] A. E. Douglas and D. Sharma, J. Opt. Soc. Am. **21**, 448 (1953).
[14] K. H. Slotta, Ber. Dtsch. Chem. Ges. **357**, 318 (1907).
[15] L. Gattermann, Liebigs Ann. Chem. **357**, 318 (1907).
[16] J. R. Wiesenfeld, Acc. Chem. Res. **15**, 110 (1982).
[17] J. C. Brock and R. T. Watsen, Chem. Phys. Lett. **71**, 371 (1980).
[18] K. Mikulecky and K.-H. Gericke, J. Chem. Phys. **96**, 7490 (1992).
[19] P. N. Clough and B. A. Thrush, Chem. Ind. 1971 (1966).
[20] R. K. Sparks, L. R. Carlson, K. Shobutake, M. L. Kowalczyk, and Y. T. Lee, J. Chem. Phys. **72**, 1401 (1980).
[21] A. C. Luntz, J. Chem. Phys. **73**, 1143 (1980).

[22] K. Mikulecky and K.-H. Gericke, Chem. Phys. **175**, 13 (1993).
[23] P. Pechukas and J. C. Light, J. Chem. Phys. **42**, 3281 (1965).
[24] P. Pechukas and J. C. Light, J. Chem. Phys. **44**, 794 (1966).
[25] J. R. Beresford and G. Hancock, Faraday Discuss. Chem. Soc. **75**, 211 (1983).
[26] A. Ben-Saul, Chem. Phys. **22**, 341 (1977).
[27] W. Forst, *Theory of Unimolekular Reactions* (Academic, New York, 1972), p. 134.
[28] D. Poppinger, L. Radom, and J. Pople, J. Am. Chem. Soc. **99**, 7806 (1977).
[29] J. W. Rabalais, J. R. McDonald, and S. P. McGlynn, J. Chem. Phys. **51**, 5103 (1969).